Elsevier Editorial System(tm) for Postharvest Biology and Technology
Manuscript Draft

Manuscript Number: POSTEC-D-14-00427

Title: Optical properties, ethylene production and softening in mango fruit

Article Type: Research Paper

Keywords: mango, maturity, ethylene, absorption, scattering, Time-resolved Reflectance Spectroscopy.

Corresponding Author: Dott Paola Eccher Zerbini,

Corresponding Author's Institution: Wageningen University

First Author: Paola Eccher Zerbini

Order of Authors: Paola Eccher Zerbini; Maristella Vanoli; Anna Rizzolo; Maurizio Grassi; Rodrigo Pimentel; Lorenzo Spinelli; Alessandro Torricelli

Abstract: Firmness decay, chlorophyll breakdown and carotenoid accumulation, controlled by ethylene, are major ripening events in mango fruit. Pigment content and structure affect the optical properties of the mesocarp, which can be measured nondestructively in the intact fruit by Time-resolved Reflectance Spectroscopy (TRS). This work aimed at finding a quantitative relation between optical properties and ethylene production rate or firmness decay in mango fruit (Mangifera indica L. cv 'Haden') from Brazil. Scattering and absorption in the 540-900 nm spectral range by TRS, ethylene production and respiration rate, and at last firmness, were measured on one day on each individual fruit of a sample covering all the range of maturity. The fruit displayed a variability which was attributed to the different biological age. Absorption spectra showed two peaks at 540 and 670 nm, corresponding respectively to the tail of carotenoid absorption and to chlorophyll-a absorption. Carotenoids increased substantially only in fruit where chlorophyll had almost disappeared. The absorptions at 540 and 670 nm, which described the maturity state of each fruit relative to the range of each wavelength, were combined in one index of biological age (biological shift factor) for each fruit and used in logistic models of ethylene increase and firmness decay respectively. The biological shift factor explained about 80% of the variability in ethylene production rate. A similar result was obtained for firmness when also scattering was added in the model. The combination of absorption at 540 and 670 nm measured by TRS in the intact fruit can be used as an effective maturity index for mango.

Suggested Reviewers:

Opposed Reviewers:

***Cover Letter**

Dear Sir,

I would like the manuscript entitled:

‘Optical properties, ethylene production and softening in mango fruit’

to be considered for publication in Postharvest Biology and Technology.

This paper reports a study on optical properties related to pigment content (absorption) and to structure (scattering) of the mango mesocarp measured nondestructively in intact fruit by Time-resolved Reflectance Spectroscopy (TRS). Optical absorption of carotenoids and chlorophyll and scattering spectra were related to ethylene production and to firmness by a model which explained 80% of the variation of the latter variables. Optical absorption and scattering at selected wavelengths measured by TRS can provide a relative assessment of the biological age of individual fruit and so manage the biological variation which is found in a batch of fruit due to their different age at harvest.

Sincerely,

Paola Eccher Zerbini

Highlights

- Both chlorophyll and carotenoids in the mesocarp are indicators of maturity in mango.
- TRS can detect pigments nondestructively by probing the mesocarp in intact fruit.
- Ethylene and firmness were related to absorption at 540 and 670 nm by logistic models.
- Both wavelengths were necessary to explain 80% of ethylene production rate variation.
- Both wavelengths and a scattering parameter explained 80% of firmness decay variation.

Optical properties, ethylene production and softening in mango fruit

Paola Eccher Zerbini[a,*], Maristella Vanoli[b,c], Anna Rizzolo[c], Maurizio Grassi[c], Rodrigo Meirelles de Azevedo Pimentel[d], Lorenzo Spinelli[e], Alessandro Torricelli[b]

[a] Horticulture and Product Physiology (Horticultural Supply Chains), Wageningen University, Droevendaalsesteeg 1, 6708 PD Wageningen, The Netherlands
[b] Dipartimento di Fisica, Politecnico di Milano, Piazza L. Da Vinci, 32 – 20133 Milano, Italy
[c] Consiglio per la Ricerca e Sperimentazione in Agricoltura – Unità di ricerca per i processi dell'industria agroalimentare (CRA-IAA), via Venezian 26 – 20133 Milano, Italy
[d] Empresa de Pesquisa Agropecuária de Minas Gerais (EPAMIG), Av. José Cândido da Silveira, 1647 - Cidade Nova, Belo Horizonte, Minas Gerais, Brasil
[e] Istituto di Fotonica e Nanotecnologie, CNR, Piazza L. Da Vinci, 32 – 20133 Milano, Italy

Corresponding author:
Paola Eccher Zerbini
E-mail: paola.zerbini@wur.nl

Abstract

Firmness decay, chlorophyll breakdown and carotenoid accumulation, controlled by ethylene, are major ripening events in mango fruit. Pigment content and structure affect the optical properties of the mesocarp, which can be measured nondestructively in the intact fruit by Time-resolved Reflectance Spectroscopy (TRS). This work aimed at finding a relation between optical properties and ethylene production rate or firmness decay in mango fruit (*Mangifera indica* L. cv 'Haden') from Brazil. Scattering and absorption in the 540–900 nm spectral range by TRS, ethylene production and respiration rate, and at last firmness, were measured on one day on each individual fruit of a sample covering all the range of maturity. The fruit displayed a variability which was attributed to the different biological age. Absorption spectra showed two peaks at 540 and 670 nm, corresponding respectively to the tail of carotenoid absorption and to chlorophyll-a absorption. Carotenoids increased substantially only in fruit where chlorophyll had almost disappeared. The absorptions at 540 and 670 nm, which described the maturity state of each fruit relative to the range of each wavelength, were

combined in one index of biological age (biological shift factor) for each fruit and used in logistic models of ethylene increase and firmness decay respectively. The biological shift factor explained about 80% of the variability in ethylene production rate. A similar result was obtained for firmness when also scattering was added in the model. The combination of absorption at 540 and 670 nm measured by TRS in the intact fruit can be used as an effective maturity index for mango.

Keywords: mango, maturity, ethylene, absorption, scattering, Time-resolved Reflectance Spectroscopy.

Abstract

Firmness decay, chlorophyll breakdown and carotenoid accumulation, controlled by ethylene, are major ripening events in mango fruit. Pigment content and structure affect the optical properties of the mesocarp, which can be measured nondestructively in the intact fruit by Time-resolved Reflectance Spectroscopy (TRS). This work aimed at finding a relation between optical properties and ethylene production rate or firmness decay in mango fruit (*Mangifera indica* L. cv 'Haden') from Brazil. Scattering and absorption in the 540–900 nm spectral range by TRS, ethylene production and respiration rate, and at last firmness, were measured on one day on each individual fruit of a sample covering all the range of maturity. The fruit displayed a variability which was attributed to the different biological age. Absorption spectra showed two peaks at 540 and 670 nm, corresponding respectively to the tail of carotenoid absorption and to chlorophyll-a absorption. Carotenoids increased substantially only in fruit where chlorophyll had almost disappeared. The absorptions at 540 and 670 nm, which described the maturity state of each fruit relative to the range of each wavelength, were combined in one index of biological age (biological shift factor) for each fruit and used in logistic models of ethylene increase and firmness decay respectively. The biological shift factor explained about 80% of the variability in ethylene production rate. A similar result was obtained for firmness when also scattering was added in the model. The combination of absorption at 540 and 670 nm measured by TRS in the intact fruit can be used as an effective maturity index for mango.

1. Introduction

1.1. Mango maturity and ripening

Mango (*Mangifera indica* L.), as other climacteric fruits, is generally harvested at the preclimacteric, mature-green stage, and its ripening process is completed in the postharvest phase. Fruit harvested in ripe condition has a better quality for direct consumption, but a shorter shelf-life. For long supply chains the maturity stage at harvest must prevent ripening during transport, while ensuring acceptable potential for subsequent ripening. Fruit harvested too early may be unable to ripen, as the ripening

ability of a fruit is acquired on the tree (Joas et al., 2012). Fruit maturity at the tree level is heterogeneous owing to variations in flowering time between branches on the same tree as well as to variability in environmental conditions of the fruit-bearing branches (Léchaudel and Joas, 2007). This variance may be seen as a disadvantage for fruit industry which looks for uniform batches of produce; however, when the variance can be recognized, it can also be managed in order to treat each fruit in the most suitable way, e.g. destining the less mature fruit to long transport and the more mature one to direct consumption in the near or gourmet markets. Therefore it is important to find some indicators of the maturity of the individual fruit. Commonly the shape and appearance of the fruit is used in practice. According to Kienzle et al. (2011), titratable acidity, mesocarp yellowness and dry matter are the most useful indices to specify harvest maturity. Exocarp color changes with maturity, but it is not well correlated to other maturity indices. Best tools to assess changes in fruit during ripening were the penetrometer, followed by flesh a^* value and total soluble solids content (Padda et al., 2011). Unfortunately all these measurements are destructive.

1.2. Ethylene, chlorophyll and carotenoids

The ripening process of climacteric fruits is regulated by genetic and biochemical events that result in changes in color, texture, aroma, nutritional content and flavor of the fruit (Giovannoni, 2004). Ethylene plays a major role in controlling these events. During ripening, ethylene production becomes autocatalytic, being stimulated by ethylene itself. Softening, change of exocarp and mesocarp color and development of volatiles are among the most obvious symptoms of ripening. During fruit ripening, chloroplasts differentiate into chromoplasts by disintegration of the thylakoid membranes and by the development of new pigment-bearing structures as observed in pepper (Camara and Brangeon ,1981) and mango (Vásquez-Caicedo et al., 2006). This process is accompanied by biochemical changes such as degradation of chlorophyll and accumulation of carotenoids, which cause the characteristic bright yellow-orange coloration of mesocarp in ripening mangoes (Vasquez-Caicedo et al., 2005). Ethylene accelerates the chlorophyll breakdown and stimulates the biosynthesis of carotenoids and their precursors (Montalvo et al., 2009; Rodrigo and Zacarias, 2007). Ethylene and carotenoids synthesis and chlorophyll degradation pathways are integrated in that they share some

common regulating factors (Lee et al., 2012; Luo et al., 2013). The most abundant carotenoids in mango are all-trans-β-carotene, all-trans-violaxanthin and 9-cis-violaxanthin. Ripe 'Haden' fruit was characterized by a high content of all-trans-β-carotene and all-trans-violaxanthin as compared to other cultivars (Ornelas-Paz et al., 2007). The concentrations of these carotenoids increased in an exponential manner during fruit ripening and were highly correlated with the color coordinate *a** (positive) and with *H*° (negative) values of the mesocarp (Ornelas-Paz et al., 2008).

1.3. Time-resolved Reflectance Spectroscopy

Time-resolved Reflectance Spectroscopy (TRS) is a nondestructive optical technique which quantifies the optical properties, i.e. the absorption (μ_a) and reduced scattering (μ_s') coefficients in the VIS-NIR wavelength range of diffusive media like biological tissue. Absorption is due to pigments present in the medium, while scattering is due to microscopic changes in refractive index caused by membranes, air, vacuoles, or organelles. TRS probes the intact fruit at a depth of 1–2 cm with no or limited influence from the skin (Cubeddu et al., 2001; Torricelli et al., 2008). It was found that the 2-3 mm green layer in the mango exocarp attenuated the intensity of the TRS signal in the 540-900 nm spectral range, but it did not affect the estimate of the optical properties of the mesocarp (Spinelli et al., 2012). The absorption spectra measured by TRS in the intact mango fruit were in agreement with the absorbance spectra of the mesocarp as assessed by a spectrophotometer on the peeled fruit (Spinelli et al., 2013). TRS absorption spectra reflected the changes in mesocarp color as *H*° was correlated negatively to μ_a540, and positively to μ_a670 (Spinelli et al., 2012; Vanoli et al., 2011a, 2013). On the contrary, the spectra measured by spectrophotometer on the intact fruit were affected by anthocyanins in the exocarp and were not useful to detect carotenoids (Spinelli et al., 2012).

Scattering spectra can be interpreted with Mie theory: under the hypothesis that the scattering centers are homogeneous spheres behaving individually, Mie theory predicts the wavelength dependence of the scattering and the relation between scattering and sphere size and density. A significant positive correlation was found between firmness and μ_s'880 in ripening 'Tommy Atkins' mangoes (Vanoli et al., 2013). The reduced scattering coefficient gave an insight into the textural properties of apple fruit: μ_s' measured at 750 and 780 nm were related to pectin composition showing a high and positive

correlation with galacturonic acid content in water soluble pectin fraction, and a negative correlation with residue insoluble pectin and protopectin index (Vanoli et al., 2009). The μ_s' measured in the range between 750 and 790 nm were also correlated to mechanical properties of fruit (firmness, stiffness, intercellular spaces) (Vanoli et al., 2007).

1.4. Biological shift factor

In the last decade, biological variation has been studied by many authors (De Ketelaere et al., 2006; Hertog, 2002; Hertog et al., 2004; Schouten et al., 2004; Tijskens et al., 2003). The concept of biological shift factor allows reducing many different aspects of variation in postharvest behaviour to that of a different biological age of individuals which share a common behaviour at constant conditions (Tijskens et al. 2005). In nectarines, μ_a670, near the chlorophyll-*a* absorption peak, was considered an index of the fruit biological age (Tijskens et al., 2007) and, converted into the biological shift factor, was successfully used to predict fruit softening rate during shelf life, and, hence, to select fruit for different market destinations (Eccher Zerbini et al., 2009). A previous work on 'Tommy Atkins' mango fruit showed that μ_a630 (related to chlorophyll-*b* content) could be used to predict softening rate, but the model explained only 70% of the variation in firmness decay rate (Pereira et al., 2010).

This work aimed at finding a quantitative relation between the optical properties of mango mesocarp, measured nondestructively by TRS, and ethylene production rate (EP) or firmness, assuming that the processes of pigment breakdown (chlorophyll) and biosynthesis (carotenoids) are related to ethylene biosynthesis.

2.Material and methods

2.1 Time-resolved Reflectance Spectroscopy

The schematic of the TRS setup developed at Politecnico di Milano and used for measurements is shown in Fig. 1 (Spinelli et al., 2012). The light source was a supercontinuum fiber laser (SC450-6W, Fianium, UK) providing white-light picosecond pulses, adjustable in power by a variable neutral-

density attenuator. A filter wheel loaded with 14 band-pass interference filters was used for spectral selection in the range 540–940 nm. Light was delivered to the sample by means of a multimode graded-index fiber. Diffuse remitted light was collected by 1 mm fiber. The light then was detected with a photomultiplier (HPM-100-50, Becker&Hickl, Germany) and the photon distribution of time-of-flight was measured by a time-correlated single-photon counting board (SPC-130, Becker&Hickl, Germany). A model for photon diffusion in turbid media was used to analyze TRS data to assess the bulk optical properties of samples (Martelli et al., 2009) to obtain the estimates of μ_a and μ_s' at each wavelength. An approximation of Mie theory: $\mu_s' = A\,(\lambda/\lambda_0)^{-B}$, where λ is wavelength, *A* the scattering coefficient at the reference wavelength λ_0= 600 nm, and *B* is a parameter related to the equivalent size of the scattering centres (Mourant et al., 1997; Nilsson et al., 1998) was used to relate μ_s' to the structural properties of the medium (density and size of scattering centres).

2.2 Fruit

Mango fruit (cv. 'Haden') harvested in a commercial orchard in Minas Gerais, Brazil, was immediately transported by plane to Milan, Italy. At arrival, 60 fruits without defects were selected and individually measured by means of the TRS set-up for the μ_a650 as the signal-to-noise ratio observed at 670 nm (i.e. on the chlorophyll-*a* peak) was too low to guarantee reliable TRS measurements. Each fruit was measured on two opposite sides and the results were averaged per fruit, then mangoes were sorted by decreasing μ_a650, i.e. increasing maturity and stored at 20°C.

After two days at 20°C, a subsample of 20 fruits, covering the whole range of μ_a650, was selected and measured for ethylene production rate and respiration. The optical properties in the 540–900 nm spectral range were measured by means of the TRS set-up on two opposite sides in the equatorial region of each intact fruit and, at the same positions, flesh firmness was assessed after all nondestructive measurements. One fruit was discarded because it was decayed.

In this paper the results relative to this subsample are reported, while the global results have been presented by Spinelli et al. (2013) and Vanoli et al. (2012).

2.3 Ethylene and respiration measurement

189 Ethylene production rate (EP) and respiration were measured by putting fruit in 1.7 L gastight glass
190 jars (one fruit per jar) for 2 h at 20°C; then, for the determination of the ethylene content, 1 mL of the
191 headspace gas was sampled and analyzed using a deactivated aluminum oxide F1 (80-100 mesh)
192 column (1/8 in × 200 cm) at a column temperature of 100°C and FID detection. Quantitative data were
193 obtained by relating the ethylene peak area to that of a 10 μL/L standard and were expressed as pmol
194 $kg^{-1}s^{-1}$. The results of four fruits were missing due to problems in the analysis.
195 For the analysis of respiratory gases (CO_2, O_2), the jar was directly connected to the MicroGC MTI
196 (model P-200, Hewlett- Packard) fitted with two columns in parallel: a MS5A column (4 m x 0.32 mm
197 ID, 30μm) at 45°C and an OV-1 column (4 m x 0.15 mm ID, 1.2 μm) at 40°C, each equipped with a
198 thermal conductivity detector. GC data were corrected for fruit mass, void volume, temperature and
199 pressure of the jar and the time of production to express CO_2 production and O_2 uptake rates as
200 nmol kg^{-1} s^{-1} in standard conditions. Respiratory quotient (RQ) was computed as the ratio between
201 CO_2 production and O_2 uptake rates.
202
203 2.4 Firmness
204 Flesh firmness was measured using a penetrometer (Instron UTM model 4301, crosshead speed 200
205 mm min^{-1}, 8 mm diameter plunger) after skin removal by a slicer, in position corresponding to the
206 TRS readings.
207
208 2.5 Ethylene production model
209 It was assumed that EP during mango ripening is autocatalytic, following a sigmoid curve increasing
210 with biological age of fruit from zero to a maximum production rate (EP_{max}):
211

212 $$EP = \frac{EP_{\max}}{1 + e^{-\Delta t_{EP}^{*}}} \qquad (1)$$

213

where Δt_{EP}* is the biological shift factor (BSF) for ethylene, which accounts for the different age of individual fruit in regard to ethylene production rate (Tijskens et al., 2005). The variability of maturity in the batch of mangoes, which were measured at one time, represents a set of different biological ages, so each individual fruit represents one biological age and will have its biological shift factor. By this model it was also assumed that all fruit in the batch, grown in the same orchard and conditions, had the same behaviour as regards EP in the course of ripening. Each fruit, with its BSF, represents a different step in the same process. Δt_{EP}* is a stochastic variable that contains all the information concerning maturity for each individual fruit in the whole batch, expressed in standardised dimensionless time (Tijsken et al., 2007). The BSF is the shift of individual fruit maturity in relation to the intermediate maturity (BSF=0) corresponding to EP equal to half of the maximum. The BSF for ethylene is an index of the fruit age in terms of its ethylene biosynthesis, which is known to increase during fruit ripening. The age of fruit can also be described in terms of the stage of chlorophyll breakdown and/or of carotenoid accumulation. Both processes characterize fruit ripening and can be assessed by absorption at 670 and 450 nm respectively. In our experiment we could not perform measurements at 450 nm, however even at 540 nm the effect of carotenoids was well appreciable (see Section 3.1). Tijskens et al. (2006) showed that μ_a670 in nectarines followed a logistic decay during ripening, both on the tree and off the tree. The concentration of carotenoids was found to increase exponentially during mango ripening (Vásquez-Caicedo et al., 2006; Ornelas-Paz et al., 2008); however, it is reasonable to assume that the increase may not be infinite and eventually a maximum will be reached. In fact preliminary analysis showed that μ_a670 followed a logistic decay also in mango, similar to that of nectarines, and μ_a540 followed a logistic but increasing trend (data not shown). Both for chlorophyll degradation and for carotenoid accumulation each fruit is characterized by its individual BSF. Since both these biochemical processes are related to ethylene biosynthesis, it can be assumed that the BSF for ethylene is linearly related to those of chlorophyll and of carotenoids. So it was assumed that the BSF for ethylene (Δt_{EP}* in Eq.1) could be expressed as a function of the measured μ_a540 and μ_a670 relatively to their range:

$$\Delta t_{EP}{}^{*} = \alpha_{540}\left(\log\left(\frac{\mu_{\mathrm{a,\,max}}^{540} - \mu_{\mathrm{a,\,0}}^{540}}{\mu_{\mathrm{a,\,0}}^{540} - \mu_{\mathrm{a,\,min}}^{540}}\right) + \beta_{540}\right) + \alpha_{670}\left(\log\left(\frac{\mu_{\mathrm{a,\,max}}^{670} - \mu_{\mathrm{a,\,0}}^{670}}{\mu_{\mathrm{a,\,0}}^{670} - \mu_{\mathrm{a,\,min}}^{670}}\right) + \beta_{670}\right) \quad (2)$$

where α_{540}, α_{670}, β_{540} and β_{670} are parameters to be estimated. The index 0 indicates the absorption measured in each fruit by TRS on the same day as EP measurement. The indices max and min indicate the maximum and minimum values ever possible (at plus and minus infinite time). They were fixed at the maximum and minimum values found in this ($\mu_{a,\max}^{540}$ and $\mu_{a,\min}^{670}$) or other ($\mu_{a,\min}^{540}$ and $\mu_{a,\max}^{670}$) experiments with mango fruit, where we could find fruit with extreme values:

$$\Delta t_{EP}{}^{*} = \alpha_{540}\cdot\left(\log\left(\frac{0.84 - \mu_{\mathrm{a,\,0}}^{540}}{\mu_{\mathrm{a,\,0}}^{540} - 0.05}\right) + \beta_{540}\right) + \alpha_{670}\cdot\left(\log\left(\frac{0.65 - \mu_{\mathrm{a,\,0}}^{670}}{\mu_{\mathrm{a,\,0}}^{670} - 0.025}\right) + \beta_{670}\right) \quad (3)$$

2.6 Firmness decay model

A similar approach was also applied to firmness. A model for firmness decay was developed by Tijskens et al. (2007). That model is used here to relate firmness to biological shift factor for firmness as assessed by μ_a540 and μ_a670. Firmness, in mango and other fruits, decays to a minimum value without reaching zero:

$$F = F_{\min} + \frac{F_{\max} - F_{\min}}{1 + e^{\Delta t_F{}^{*}}} \quad (4)$$

where F is firmness and $F_{\max}$ and $F_{\min}$ its maximum and minimum values ever possible (at minus and plus infinite time). The biological shift factor Δt_F* has the same meaning as in the case of ethylene: it accounts for the different age of individual fruit in regard to firmness decay. Firmness decay during ripening parallels chlorophyll degradation and carotenoid accumulation, as all these processes are dependent on ethylene, so it can be assumed that the BSF for firmness (Δt_F* in Eq.4) is linearly related to the BSFs of chlorophyll and of carotenoids and can be expressed as a function of the measured

absorptions at 540 and 670 nm (Eq. 5). In the Eq. 5 also two terms related to scattering (the Mie's *A* and *B* estimated from scattering spectra) were added, assuming that firmness decay is paralleled by a change in scattering:

$$\Delta t_F^{\,*} = \alpha_{F,540}\left(\log\left(\frac{\mu_{a,\max}^{540}-\mu_{a,0}^{540}}{\mu_{a,0}^{540}-\mu_{a,\min}^{540}}\right)+\beta_{F,540}\right)+\alpha_{F,670}\left(\log\left(\frac{\mu_{a,\max}^{670}-\mu_{a,0}^{670}}{\mu_{a,0}^{670}-\mu_{a,\min}^{670}}\right)+\beta_{F,670}\right)+k_A A+k_B B \quad (5)$$

where μ_a symbols and values are the same indicated for Eq. 2 and 3, while $\alpha_{F,540}$, $\alpha_{F,670}$, $\beta_{F,540}$, $\beta_{F,670}$, k_A and k_B are parameters to be estimated.

2.7 Statistical analysis

EP and firmness data were analyzed by non-linear regression (PROC NLIN, SAS/STAT, SAS Institute Inc., Cary, NC, 2002) based on model (1) combined with Eq. (3) for EP, and on model (4) combined with Eq. (5) for firmness. In this way, EP and firmness were represented as functions of fruit maturity at time of measurement, as assessed by selected optical properties.

3. Results

3.1. Optical properties

Absorption spectrum in the range 540-900 nm showed two main peaks (Fig. 2). The variation was very high in the 540-580 nm range, near the carotenoid absorption peak, while it was still remarkable, but less high in the 650-690 nm range, in the region of chlorophyll-*a* absorption. There was also a slight contribution of water absorption in the 800-900 nm region. In Fig. 2, a high absorption at 670 nm corresponded to a low absorption at 540 nm. With increasing absorption at 540 nm, that at 670 nm decreased. Only when the absorption at 540 nm was very high, the tail of this peak affected the absorption at 670 nm, which increased slightly. At wavelengths higher than 730 nm there were no differences between fruits. The relation between μ_a540 and μ_a670 is made clear in Fig. 3, left. Absorption of carotenoids (μ_a540) remained around 0.2 cm^{-1} as long as chlorophyll absorption (μ_a670)

291 was present. When chlorophyll disappeared, μ_a670 did not become zero, but remained around 0.03
292 cm^{-1}, which can be ascribed to the background absorption due to the many absorbing compounds in
293 the tissue, other than chlorophyll. Carotenoids (μ_a540) increased only where μ_a670 was below 0.04
294 cm^{-1}.
295 Scattering (Fig. 2) decreased with increasing wavelength, as predicted by Mie theory. The range of
296 variation was quite high among fruit, as regards both the average level (related to parameter *A*) and the
297 slope (related to parameter *B*) (Fig. 3, right).
298
299 3.2. Respiration
300 Oxygen uptake rate ranged between 360 and 570 nmol $kg^{-1}s^{-1}$. The range of CO_2 production rate was
301 slightly higher (400-670 nmol $kg^{-1}s^{-1}$). Respiration data in relation to μ_a540 show that CO_2 production
302 was similar to O_2 uptake when μ_a540 was low, but with μ_a540>0.8 cm^{-1} the CO_2 production rate was
303 higher than oxygen uptake rate (Fig. 4 left). This was reflected in the respiratory quotient, which
304 increased above 1 when μ_a540 was high (Fig.4 right).
305
306 3.3. Ethylene production rate.
307 EP ranged from 0.1 to 0.5 pmol $kg^{-1}s^{-1}$. EP increased with increasing μ_a540, and with decreasing μ_a670
308 (Fig. 5). The results of modelling EP in function of maturity (expressed as biological shift factor
309 derived from μ_a540 and μ_a670) are reported in Table 1 and Fig. 6. The β parameters were not
310 significant so they were dropped from the model. The approximate standard error was low for all the
311 parameters. The estimated EP_{max} was similar to the measured maximum EP (0.496 pmol kg^{-1} s^{-1}). The
312 coefficients α_{540} and α_{670} were not correlated, and had obviously opposite sign, as μ_a540 increased and
313 μ_a670 decreased with increasing EP. This model explained 80% of the variation of EP in the batch of
314 fruit.
315 The same model was run considering only one wavelength at a time: when only μ_a540 or μ_a670 was
316 considered, R^2_{adj} became 0.61 and 0.49 respectively, indicating that both wavelengths should be
317 considered together to obtain a better index of fruit age in relation to ethylene biosynthesis.
318

319 3.4 Firmness

320 Firmness indicated that most fruit was in an advanced maturity stage (Fig.7). Even if firmness varied
321 from 5 to 70 N, the majority of the mangoes had firmness lower than 20 N, which is characteristic of
322 ready to eat or ripe fruit. Firmness decreased with decreasing $\mu_a 670$, and was already low when $\mu_a 540$
323 increased above 0.2 cm^{-1}.

324 The results of modelling firmness in function of maturity as assessed by absorption at 540 and 670 and
325 by scattering are reported in Table 2 and Fig. 8. The β_F parameters and k_A were not significant and
326 were omitted. To avoid over parameterization, parameters F_{max} and F_{min} were fixed at the maximum
327 and minimum firmness measured, and $\alpha_{F,540}$ was fixed at –1.4, based on some preliminary calculations.
328 The approximate standard error of k_B was relatively high, but the presence of the scattering parameter
329 *B* in the model raised the adjusted R^2 to 0.80, while without it the R^2_{adj} was lower (0.75).
330 If either wavelength was omitted from the model, R^2_{adj} was obviously lower; when only $\mu_a 670$ was
331 used, k_B was not significant, and hence also *B* could be omitted as its effect in this restricted model
332 was near zero (R^2_{adj}=0.49), while using only $\mu_a 540$ the model could not fit, unless also *B* was
333 considered (R^2_{adj}=0.58).

334

335

336 **4. Discussion**

337 4.1. Optical properties

338 The most interesting features were absorptions related to the main pigments in the fruit, i.e.
339 chlorophyll and carotenoids, which decrease and increase respectively with fruit ripening, as already
340 found in other mango cultivars (Spinelli et al., 2012). The differences of absorption in fruit could be
341 attributed mainly to a different content of chlorophyll (670 nm) and of carotenoids (540 nm). We
342 found that $\mu_a 540$ was higher than 0.3 cm^{-1} only in fruit with $\mu_a 670$ lower than 0.04 cm^{-1}. The different
343 content was assumed to be due to a different biological age of fruit, which had undergone a more or
344 less advanced stage of ripening at the time of examination. With this assumption, it seems that
345 carotenoids increased substantially only when chlorophyll had almost disappeared. Pigments in mango
346 mesocarp were measured by Kienzle et al. (2011, 2012) who found that, during postharvest storage,

chlorophyll *a* and *b* decreased from 3.3 and 2.2 mg hg^{-1} DW, respectively, to not detectable, while all-*trans*-β-carotene increased from 0.4 to 4.9 mg hg^{-1} DW; interestingly, the carotene increased only when chlorophyll was very low or not detectable, in accordance with our results. The mechanism of this synchronization between chlorophyll degradation and carotenoid accumulation has been particularly studied in tomato. STAY-GREEN (SGR) proteins, which play important roles in the regulation of chlorophyll degradation, can also regulate and inhibit lycopene and β-carotene accumulation through direct interaction with phytoene syntase, a key carotenoid synthetic enzyme (Luo et al., 2013). It seems that high levels of SGR induce chlorophyll breakdown, while carotenoid accumulation is inhibited, until the SGR decreases so allowing carotenoid synthesis and plastid conversion. Synchronization and balance between chlorophyll breakdown and lycopene accumulation have been studied at a quantitative level using a kinetic model by Schouten et al. (2014), who found that they depend on temperature and cultivar. At microscopic level, Vasquez-Caicedo et al. (2006) found a very dynamic interconversion of the plastid structures in the mango mesocarp tissue (cv 'Tommy Atkins'), where no sequential pattern could be clearly established between chloroplasts and chromoplasts. In contrast, in our study, optical absorption measurements, which respond to pigment concentration, appeared to show a clear sequence in that the increase of μ_a540 only occurred after the complete decrease of μ_a670.

As regards scattering, the differences in μ_s' reflect the changes occurred in the mesocarp structure due to the mango softening. A decrease of scattering spectra of 'Tommy Atkins' mangoes, as well as of the parameter related to density of the scatterers was found during shelf life (Vanoli et al., 2013). Softening is due the enzymatic cell wall breakdown which may decrease the density of the scattering particles in the mesocarp so leading to less scattering events in the tissue, as found also in tomatoes, plums and apples (Qin and Lu, 2008; Seifert et al., 2014; Vanoli et al., 2011b). This suggests that fruit with lower μ_s' had a more advanced cell wall breakdown.

4.2. Respiration and ethylene production rate.

The values of oxygen uptake, CO_2 production and EP rates were similar to those reported in literature (Lalel et al., 2003; Zaharah and Singh, 2011; Zheng et al., 2007). The respiratory quotient in normal

375 aerobic conditions is around 1 (0.8 to 1.2, depending on the substrate used for energy production). A
376 higher value suggests a change from aerobic to anaerobic respiration, which occurs when oxygen in
377 the tissue is insufficiently available so that the energy requirements cannot be fulfilled. This may occur
378 in climacteric fruit when ethylene triggers many simultaneous ripening processes which require
379 energy, and at the same time the modifications and breakdown of cell walls and membranes can
380 reduce the permeability to gases. It can be assumed that fruit in this condition was already in the
381 overripe, senescent phase.
382
383 4.3. Modelling
384 The model for EP in function of μ_a540 and μ_a670 explained 80% of the variation of EP in the batch of
385 fruit. The model for firmness in function of μ_a540, μ_a670 and Mie's *B* gave a similar result, despite
386 softening already occurred at a certain extent in the batch of fruit. This confirmed the assumption that
387 there was a common behaviour as regards clorophyll degradation, carotenoid accumulation, ethylene
388 biosynthesis and softening among mango fruit grown in the same orchard: the individual differences
389 of maturity were different steps in the same process, and were taken into account by the biological
390 shift factors Δt_{EP}* and Δt_F* for ethylene and firmness respectively. Both Δt*s indicate that most fruits,
391 having a positive biological shift factor, were beyond the intermediate maturity corresponding to the
392 inflection point of the curve. To express Δt* in time dimension, this variable should be divided by the
393 range and by the rate constant at the desired temperature. However the latter information is missing,
394 having performed the experiment in one time. Further research is under way to study EP and firmness
395 decay rate in time.
396 The models show that both wavelengths should be considered together to obtain a better index of fruit
397 age in relation to ethylene biosynthesis and firmness. In fact the sequence of carotenoid accumulation
398 following the chlorophyll breakdown makes the two processes little overlapping and almost mutually
399 exclusive (Fig. 3 left), so that, depending on the fruit age, either one is prevalent. The synchronization
400 between variation in μ_a540 (carotenoids) and μ_a670 (chlorophyll) and EP or firmness could be
401 explained by the manifold effects of SGR proteins (see 4.1), which affect also ethylene signal
402 transduction by altering the expression of ethylene receptor genes and ethylene induced genes, such as

403 *polygalacturonase* and *pectinesterase* (Luo et al., 2013), which have important effects on fruit texture
404 and firmness during ripening.
405
406 **4. Conclusions**
407 The measurement of absorption coefficients by TRS allowed detecting the ripening state of each fruit,
408 by assessing the extent of chlorophyll decay and carotenoid accumulation through μ_a670 and μ_a540
409 respectively, in a nondestructive way. The optical properties, respiration, EP and firmness all showed
410 that the fruit displayed a variability of ripening stages, with some fruit definitely ripe or overripe.
411 Carotenoids increased substantially only in fruit where chlorophyll had almost disappeared. The
412 absorptions at the two wavelengths 540 and 670 nm, combined in a logistic model, defined an index of
413 biological age (biological shift factor) of each fruit which explained about 80% of the variability in the
414 ethylene production rate. A similar result was obtained for firmness when also scattering was added in
415 the model. The combination of optical absorption and scattering at selected wavelength measured by
416 TRS in the intact mango provides a relative assessment of the biological age of individual fruit
417 (maturity index) that can be used to manage the biological variation found in a batch of fruit due to
418 their different age at harvest.
419
420 **Acknowledgements**
421 This work was partially supported by Regione Lombardia (Italy) and Region Minas Gerais (Brazil)
422 (Progetto di Cooperazione Scientifica e tecnologica "Approccio multidisciplinare per l'innovazione
423 della filiera di frutti tropicali – TROPICO" ID 17077, Rif.n° AGRO-16).
424
425
426 **References**
427 Camara B., Brangeon J. 1981. Carotenoid metabolism during chloroplast to chromoplast
428 transformation in Capsicum annuum fruit. Planta 151: 359-364.

429 Cubeddu, R., D'Andrea, C., Pifferi, A., Taroni, P., Torricelli, A., Valentini, G., Dover, C., Johnson,
430 D., Ruiz-Altisent, M., Valero, C., 2001. Nondestructive quantification of chemical and physical
431 properties of fruits by time-resolved reflectance spectroscopy in the wavelength range 650–1000
432 nm. Appl. Opt., 40, 538–543.

433 De Ketelaere, B., Stulens, J., Lammertyn, J., Cuong, N.V., De Baerdemaeker, J., 2006. A
434 methodological approach for the identification and quantification of sources of biological variance
435 in postharvest research. Postharvest Biol. Technol. 39, 1–9.

436 Eccher Zerbini, P., Vanoli, M., Rizzolo, A., Jacob, S., Torricelli, A., Spinelli, L., Schouten, R.E.,
437 2009. Time-resolved Reflectance Spectroscopy as a management tool in the fruit supply chain: an
438 export trial with nectarines. Biosyst. Eng., 102, 360–363.

439 Giovannoni J.J. 2004. Genetic regulation of fruit development and ripening. Plant Cell 16(Suppl):
440 S170–S180.

441 Hertog, M.L.A.T.M., 2002. The impact of biological variation on postharvest population dynamics.
442 Postharvest Biol. Technol. 26, 253–263.

443 Hertog, M.L.A.T.M., Lammertyn, J., Desmet, M., Scheerlinck, N., Nicolaï, B.M., 2004. The impact of
444 biological variation on postharvest behaviour of tomato fruit. Postharvest Biol. Technol. 34, 271–
445 284.

446 Joas, J., Vulcain, E., Desvignes, C., Morales E., Léchaudel M. 2012. Physiological age at harvest
447 regulates the variability in postharvest ripening, sensory and nutritional characteristics of mango
448 (Mangifera indica L.) cv. Coghshall due to growing conditions. J Sci Food Agric.92(6):1282-90.

449 Kienzle, S. , Sruamsiri, P. , Carle, R. , Sirisakulwat, S. , Spreer, W., Neidhart, S. 2011. Harvest
450 maturity specification for mango fruit (Mangifera indica L. 'Chok Anan') in regard to long supply
451 chains. Postharvest Biology and Technology, 61 (1): 41-55.

452 Kienzle S., Sruamsiri P., Carle R., Sirisakulwat S., Spreer W., Neidhart S. 2012. Harvest maturity
453 detection for 'Nam Dokmai #4' mango fruit (Mangifera indica L.) in consideration of long supply
454 chains. Postharvest Biol Technol 72: 64-75.

455 Lalel, H. D. J., Singh, Z., and Tan, S. C. 2003. Aroma volatiles production during fruit ripening of
456 'Kensington Pride' mango. Postharvest Biol. Technol. 27: 323–336.

457 Léchaudel M. and Joas J, 2007. An overview of preharvest factors influencing mango fruit growth,
458 quality and postharvest behaviour. Braz J Plant Physiol 19:287–298.

459 Lee, J.M. , Joung, J.-G. , McQuinn, R. , Chung, M.-Y. , Fei, Z., Tieman, D. , Klee, H. , Giovannoni, J.
460 2012. Combined transcriptome, genetic diversity and metabolite profiling in tomato fruit reveals
461 that the ethylene response factor SlERF6 plays an important role in ripening and carotenoid
462 accumulation. Plant Journal, 70 (2), pp. 191-204.

463 Luo, Z., Zhang, J., Li, J., Yang, C., Wang, T., Ouyang, B., Li, H., Giovannoni, J. , Ye, Z. 2013. A
464 STAY-GREEN protein SlSGR1 regulates lycopene and β-carotene accumulation by interacting
465 directly with SlPSY1 during ripening processes in tomato. New Phytologist, 198 (2), pp. 442-452.

466 Martelli, F., Del Bianco, S., Ismaelli, A., Zaccanti, G., 2009. Light Propagation through Biological
467 Tissue and Other Diffusive Media: Theory, Solutions, and Software. Washington: SPIE Press.

468 Montalvo, E. , Adame, Y. , García, H.S. , Tovar, B. , Mata, M. 2009. Changes of sugars, β-carotene
469 and firmness of refrigerated Ataulfo mangoes treated with exogenous ethylene. Journal of
470 Agricultural Science, 147 (2), pp. 193-199.

471 Mourant J R, Fuselier T, Boyer J, Johnson T M and Bigio I J, 1997. Predictions and measurements of
472 scattering and absorption over broad wavelength ranges in tissue phantoms. Applied Optics, 36,
473 949-957.

474 Nilsson M K, Sturesson C, Liu D L and Andersson-Engels S, 1998. Changes in spectral shape of
475 tissue optical properties in conjunction with laser-induced thermotherapy. Applied Optics, 37,
476 1256-1267.

477 Ornelas-Paz J. de J., Yahia, E. M., Gardea, A. A. 2007. Identification and quantification of
478 xanthophyll esters, carotenes and tocopherols in the fruit of seven Mexican mango cultivars by
479 liquid chromatography-APcI+-time-of-flight mass spectrometry. Journal of Agriculture and Food
480 Chemistry, 55, 6628–6635.

481 Ornelas-Paz J. de J., Yahia, E. M., Gardea, A. A. 2008. Changes in external and internal color during
482 postharvest ripening of 'Manila' and 'Ataulfo' mango fruit and relationship with carotenoid content
483 determined by liquid chromatography-APcI+-time-of-flight mass spectrometry. Postharvest
484 Biology and Technology, 50, 145-152.

485 Padda, S.M., do Amarante, C.V.T., Garcia, R.M., Slaughter, D.C., Mitcham, E.M., 2011. Methods to
486 analyze physicochemical changes during mango ripening: A multivariate approach. Postharvest
487 Biol. Tec., 62, 267–274.

488 Pereira, T., Tijskens, L.M.M., Vanoli, M., Rizzolo, A., Eccher Zerbini, P., Torricelli, A., Spinelli, L.,
489 Filgueiras, H., 2010. Assessing the harvest maturity of brazilian mangoes. Acta Hort., 880, 269–
490 276.

491 Qin J, Lu R. (2008). Measurement of the optical properties of fruits and vegetables using spatially
492 resolved hyperspectral diffuse reflectance imaging technique. Postharvest Biology and Technology
493 49, 355−365.

494 Rodrigo, M.J., Zacarias, L. 2007. Effect of postharvest ethylene treatment on carotenoid accumulation
495 and the expression of carotenoid biosynthetic genes in the flavedo of orange (Citrus sinensis L.
496 Osbeck) fruit. Postharvest Biology and Technology, 43 (1), pp. 14-22.

497 Schouten, R.E., Jongbloed, G., Tijskens, L.M.M., van Kooten, O., 2004. Batch variability and cultivar
498 keeping quality of cucumber. Postharvest Biol. Technol. 32, 299–310.

499 Schouten R.E., Farneti B., Tijskens L.M.M., Alarcón A.A., Woltering E.J. 2014. Quantifying lycopene
500 synthesis and chlorophyll breakdown in tomatofruit using remittance VIS spectroscopy.
501 Postharvest Biol. Technol. 96: 53–63.

502 Seifert B., Zude M., Spinelli L., Torricelli A. 2014. Optical properties of developing pip and stone
503 fruit reveal underlying structural changes. Physiologia Plantarum. DOI: 10.1111/ppl.12232.

504 Spinelli L., A. Rizzolo, M. Vanoli, M. Grassi, P. Eccher Zerbini, R. M. A. Pimentel, A. Torricelli.
505 2012. Optical properties of pulp and skin in Brazilian mangoes in the 540–900 nm spectral range:
506 implication for non-destructive maturity assessment by time-resolved reflectance spectroscopy.

507 Proceedings of the 3rd CIGR International Conference of Agricultural Engineering (CIGR-
508 AgEng2012), Valencia, Spain, 8-12 July 2012, ISBN 84-615-9928-4 (Pen-drive).

509 Spinelli L., Rizzolo A., Vanoli M., Grassi M., Eccher Zerbini P., Pimentel R.M.A., Torricelli A. 2013.
510 Nondestructive assessment of fruit biological age in Brazilian mangoes by time-resolved
511 reflectance spectroscopy in the 540–900 nm spectral range. InsideFood Symposium, 9-12 April
512 2013, Leuven, Belgium. Book of Proceedings.
513 http://www.insidefood.eu/INSIDEFOOD_WEB/UK/WORD/proceedings/027P.pdf

514 Tijskens, L.M.M., Konopacki, P., Simčič, M., 2003. Biological variance, burden or benefit?
515 Postharvest Biol. Technol. 27, 15–25.

516 Tijskens, L.M.M., Heuvelink, E., Schouten, R.E., Lana, M.M., van Kooten, O., 2005. The biological
517 shift factor. Biological age as a tool for modelling in pre- and postharvest horticulture. Acta Hortic.
518 687, 39–46.

519 Tijskens, L.M.M., Eccher Zerbini, P., Vanoli, M., Jacob, S., Grassi, M., Cubeddu, R., Spinelli, L.,
520 Torricelli, A., 2006. Effects of maturity on chlorophyll related absorption in nectarines, measured
521 by non-destructive time-resolved reflectance spectroscopy. Int. J. Postharvest Technol. Innov. 1,
522 178–188.

523 Tijskens, L.M.M., Eccher Zerbini, P., Shouten, R.E., Vanoli, M., Jacob, S., Grassi, M., Cubeddu, R.,
524 Spinelli, L., Torricelli, A., 2007. Assessing harvest maturity in nectarines. Postharvest Biol. Tech.,
525 45, 204–213.

526 Torricelli, A., Spinelli, L., Contini, D., Vanoli, M., Rizzolo, A., Eccher Zerbini, P., 2008. Time-
527 resolved reflectance spectroscopy for non-destructive assessment of food quality. Sens. &
528 Instrumen. Food Qual., 2, 82–89.

529 Vanoli M., Rizzolo A., Grassi M., Zanella A., Torricelli A., Spinelli L., Eccher Zerbini P. 2007.
530 Relationship between scattering properties as measured by Time-resolved Reflectance
531 Spectroscopy and quality in apple fruit. 3rd CIGR Section VI International Symposium on Food

and Agricultural Products: Processing and Innovations, 24-26 September 2007, Naples (Italy). CD-ROM Proceedings pp 13.

Vanoli M, Eccher Zerbini P, Spinelli L, Torricelli A, Rizzolo A. 2009. Polyuronide content and correlation to optical properties measured by time-resolved reflectance spectroscopy in 'Jonagored' apples stored in normal and controlled atmosphere. Food Chem., 115: 1450−1457.

Vanoli, M., Pereira, T., Grassi, M., Spinelli, L., Filgueiras, H., Tijskens, L.M.M., Rizzolo, A., Torricelli, A., 2011a. Changes in pulp colour during postharvest ripening of Tommy Atkins mangoes and relationship with optical properties measured by time-resolved reflectance spectroscopy. 6th CIGR, Section VI, International Symposium "Towards a Sustainable Food Chain-Food Process, Bioprocessing and Food Quality Management", April 18-20, 2011, Nantes, France. CD-ROM Proceedings, ISBN 978-2-7466-3203-5.

Vanoli M., Rizzolo A., Grassi M., Farina A., Pifferi A., Spinelli L., Torricelli A. 2011b. Time-resolved reflectance spectroscopy nondestructively reveals structural changes in 'Pink Lady®' apples during storage. Procedia Food Science: 81-89.

Vanoli, A. Rizzolo, M. Grassi, R. M. A. Pimentel, P. Eccher Zerbini, L. Spinelli, A. Torricelli. 2012. Valutazione non distruttiva dell'età biologica di mango brasiliani mediante spettroscopia VIS/NIR risolta nel tempo. NIR ITALIA 2012 - 5° Simposio Italiano di Spettroscopia NIR, Atti del Simposio, 26-28 Settembre 2012, AGRIPOLIS, Legnaro, Italy, pp 113-118.

Vanoli M., Rizzolo A., Grassi M., Spinelli L., Eccher Zerbini P., Pimentel R.M.A. and Torricelli, A. 2013. Quality of Brazilian mango fruit in relation to optical properties non-destructively measured by time-resolved reflectance spectroscopy.In: Bellon-Maurel V., Williams P., Downey G. (Eds) NIR2013 Proceedings, 2-7 June 2013, La Grande-Motte, France, pp 177-181.

Vásquez-Caicedo, A. L., Sruamsiri, P., Carle, R., Neidhart, S. 2005. Accumulation of all-*trans*-*β*-carotene and its 9-*cis* and 13-*cis* stereoisomers during postharvest ripening of nine Thai mango cultivars. J Agric Food Chem 53: 4827-4835.

557 Vásquez-Caicedo A. L., Heller A., Neidhart S., Carle R. 2006. Chromoplast morphology and β-
558 carotene accumulation during postharvest ripening of mango cv. ‘Tommy Atkins'. J Agric Food
559 Chem 54 (16): 5769-5776.

560 Zaharah, S.S., Singh, Z., 2011. Mode of action of nitric oxide in inhibiting ethylene biosynthesis and
561 fruit softening during ripening and cool storage of ‘Kensington Pride’ mango. Postharvest Biol
562 Technol 62: 258–266.

563 Zheng, X., Tian, S., Gidley, M.J., Yue, H., Li, B., 2007. Effects of exogenous oxalic acid on ripening
564 and decay incidence in mango fruit during storage at room temperature. Postharvest Biol Technol
565 45: 281–287.

566

567 **Tables**

568 Table 1. Parameters of the non-linear regression model for ethylene production rate in function of

569 μ_a540 and μ_a670 (Eq. 1 and 3).

570

Parameter	Estimate	Approx. Std Error	Approx. 95% Confidence Limits	
EP_{max}	0.48	0.05	0.38	0.58
α_{540}	-0.73	0.16	-1.08	-0.38
α_{670}	0.37	0.11	0.14	0.61
R^2_{adj}	0.80			

571

572

573

574 Table 2. Parameters of the non-linear regression model for firmness in function of μ_a540 and μ_a670

575 and of Mie's B (Eq. 4 and 5) . F_{max}, F_{min} and $\alpha_{F,540}$were fixed.

576

Parameter	Estimate	Approx. Std Error	Approx. 95% Confidence Limits	
F_{max}	65	-		
F_{min}	5	-		
$\alpha_{F,540}$	-1.4	-		
$\alpha_{F,670}$	0.53	0.14	0.23	0.83
k_B	5.41	1.29	2.69	8.12
R^2_{adj}	0.80			

577

578

579 **Figure captions**

580

581 Fig. 1. Scheme of the TRS instrumental setup. TCSPC: time-correlated single-photon counting board;
582 SYNC: synchronization signal; CFD: constant fraction discriminator.

583 Fig. 2. Absorption (left) and scattering (right) spectra measured on 20 mango fruit cv 'Haden'
584 covering the whole range of maturity.

585 Fig. 3. Relation between μ_a540 and μ_a670 (left) and Mie's *A* and *B* (right) in mangoes cv 'Haden'.

586 Fig. 4. Oxygen uptake and CO_2 production rate (left) in mango fruit cv 'Haden' and their respiratory
587 quotient (right) in function of μ_a540 .

588 Fig. 5. Ethylene production rate in function of μ_a540 (left) and μ_a670 (right).

589 Fig. 6. Measured data (diamonds) and predicted ethylene production rate (line) in function of
590 biological shift factor (Δt_{EP}*) as assessed by μ_a540 and μ_a670 according to model (eq. 1 and 3) and
591 parameters in Table 1.

592 Fig. 7. Firmness in function of μ_a540 (left) and μ_a670 (right).

593 Fig. 8. Measured data (diamonds) and predicted firmness decay (line) in function of the biological
594 shift factor (Δt_F*) as assessed by μ_a540, μ_a670 and Mie's B, according to model (eq. 4 and 5) and
595 parameters in Table 2.

596

597

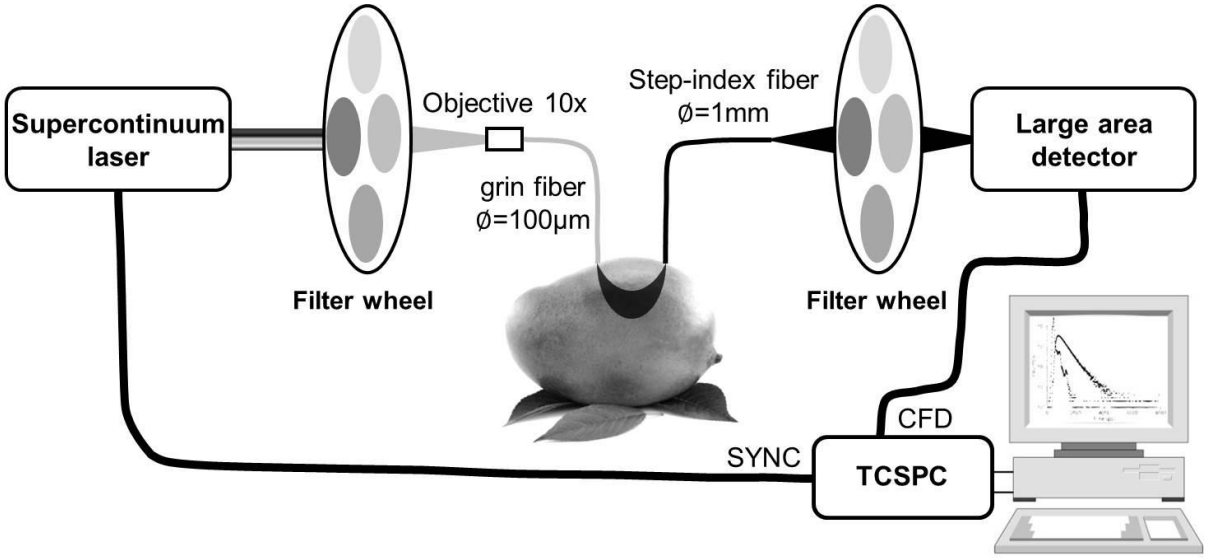

Fig. 1. Scheme of the TRS instrumental setup. TCSPC: time-correlated single-photon counting board; SYNC: synchronization signal; CFD: constant fraction discriminator.

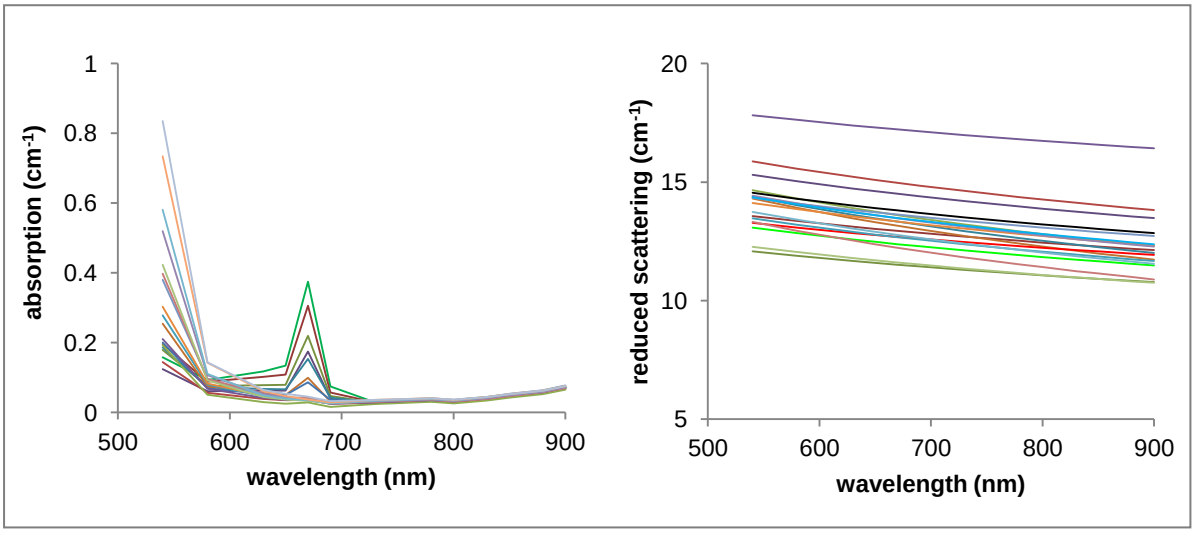

Fig. 2. Absorption (left) and scattering (right) spectra measured on 20 mango fruit cv 'Haden' covering the whole range of maturity.

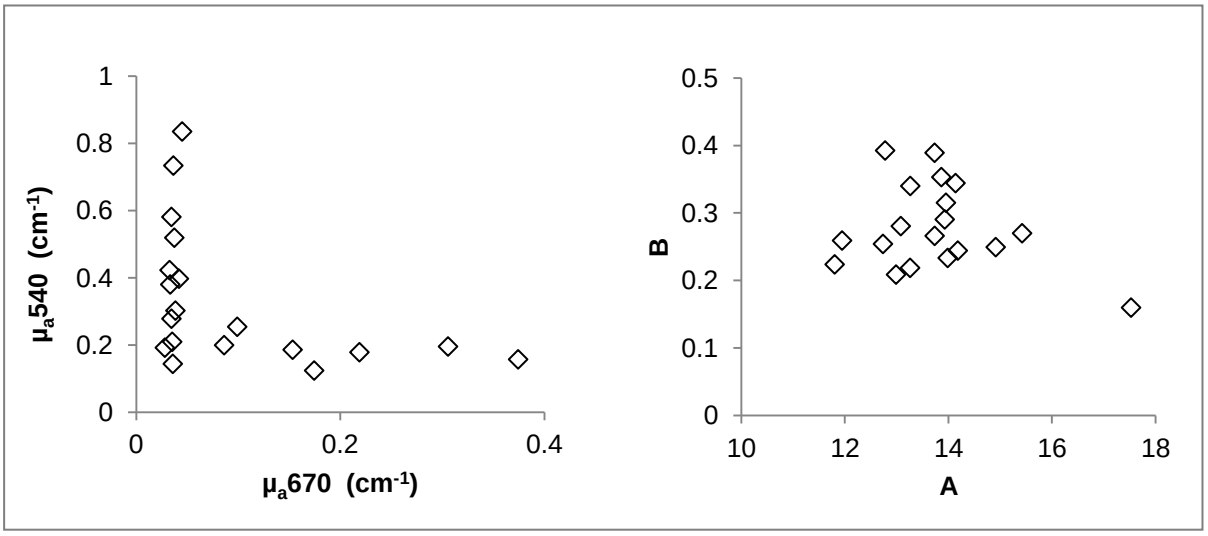

Fig. 3. Relation between μ_a540 and μ_a670 (left) and Mie's A and B (right) in mangoes cv 'Haden'.

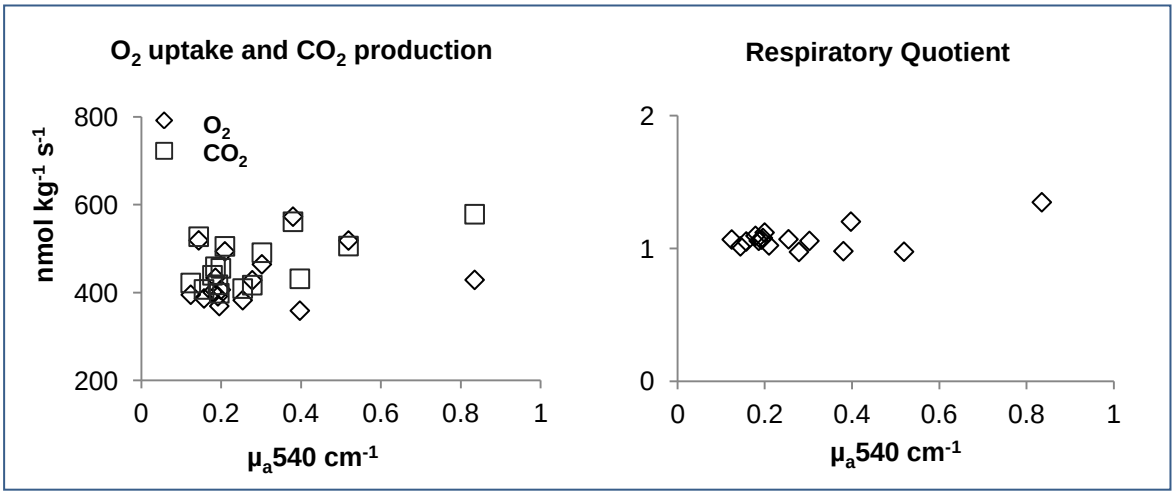

Fig. 4. Oxygen uptake and CO_2 production rate (left) in mango fruit cv 'Haden' and their respiratory quotient (right) in function of μ_a540.

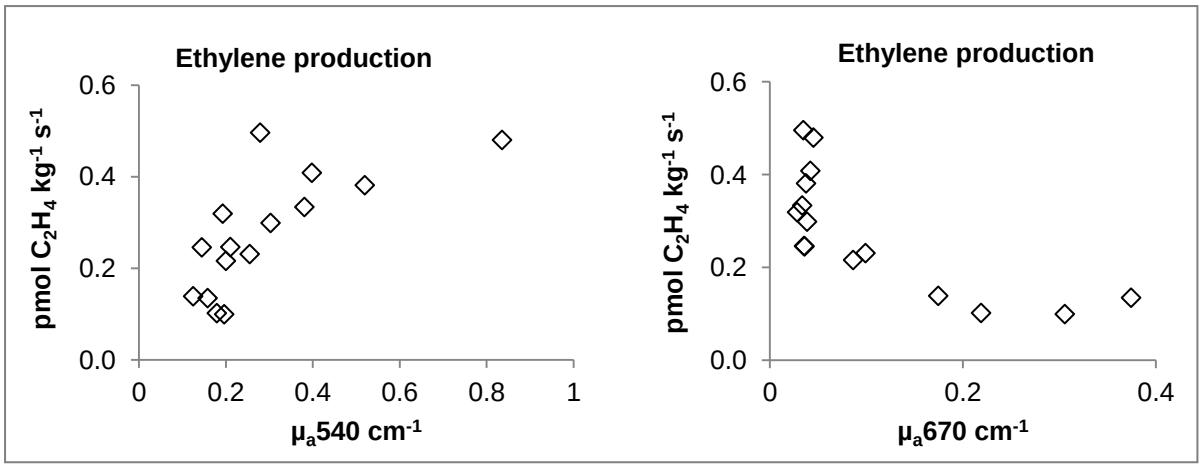

624

625

626 Fig. 5. Ethylene production rate in function of μ_a540 (left) and μ_a670 (right).

627

628

629

630

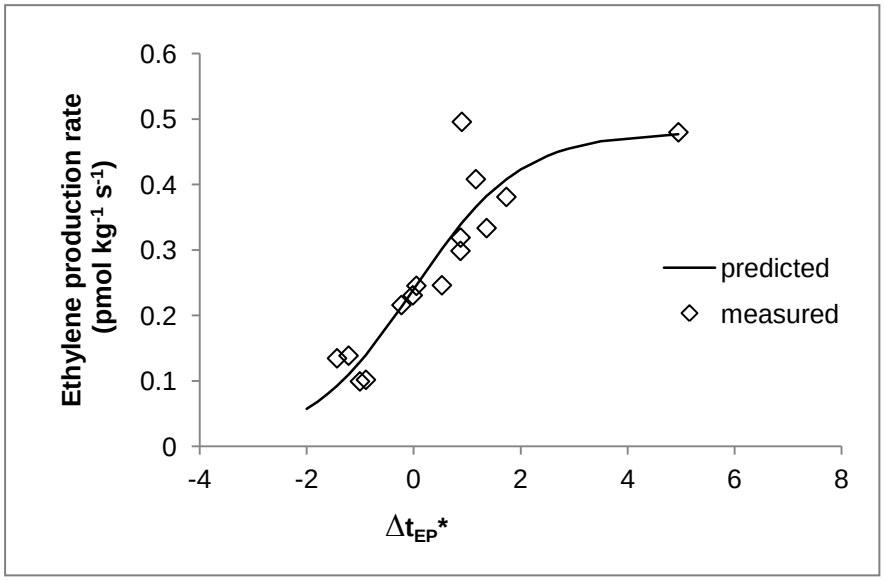

631

632

633 Fig. 6. Measured data (diamonds) and predicted ethylene production rate (line) in function of

634 biological shift factor (Δt_{EP}*) as assessed by μ_a540 and μ_a670 according to model (eq. 1 and 3) and

635 parameters in Table 1.

636

637

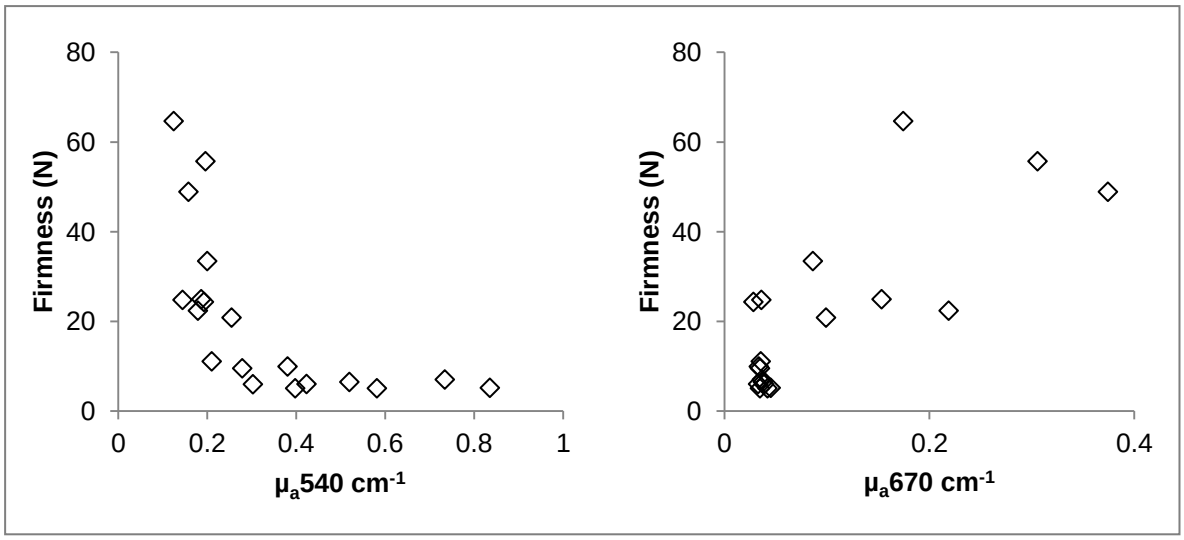

638

639

640 Fig. 7. Firmness in function of μ_a540 (left) and μ_a670 (right).

641

642

643

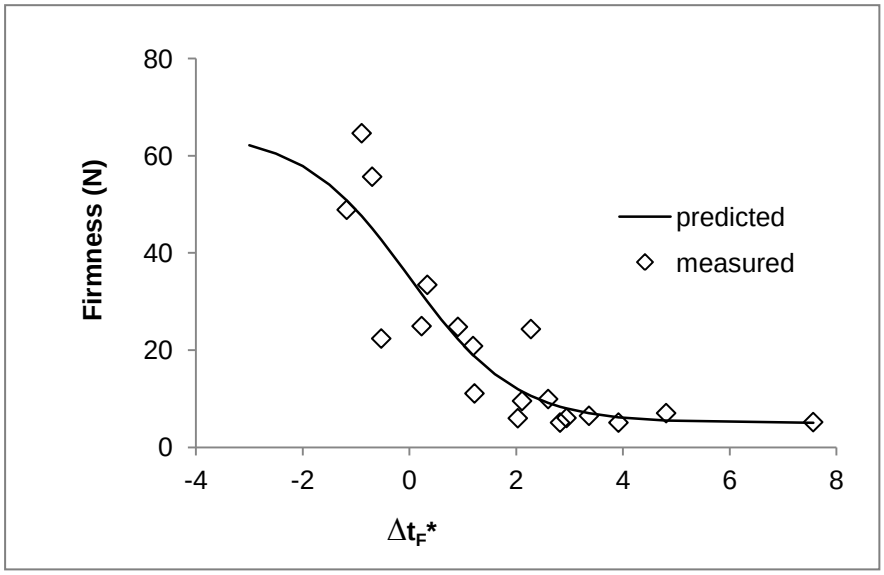

644

645

646 Fig. 8. Measured data (diamonds) and predicted firmness decay (line) in function of the biological

647 shift factor (Δt_F*) as assessed by μ_a540, μ_a670 and Mie's B, according to model (eq. 4 and 5) and

648 parameters in Table 2.

649

***Potential Reviewers List**

Potential reviewers list

Manuela Zude mzude@atb-potsdam.de

Phul P. Subedi p.subedi@cqu.edu.au